

Searching for the $0\nu\beta\beta$ decay with the SuperNEMO demonstrator

February 20, 2020

Contents

Contents	2
Introduction	5
1 Phenomenology of particle physics	6
1.1 The Standard Model of particle physics	6
1.1.1 Bosons	6
1.1.2 Fermions	6
1.1.3 $2\nu\beta\beta$ decay	6
1.1.4 Where the Standard Model ends	6
1.2 Going beyond the Standard Model with neutrinos	6
1.2.1 Neutrino flavors and oscillations	6
1.2.2 Neutrino masses and nature	6
1.2.3 Other searches beyond the Standard Model with neutrinos	6
2 $0\nu\beta\beta$ experiment status	7
2.1 Experimental design criteria	7
2.1.1 Aspects of the nuclear matrix elements	8
2.1.2 Quenching	8
2.2 $0\nu\beta\beta$ direct search experiments	8
2.2.1 Semiconductors	8
2.2.2 Bolometers	9
2.2.3 Time projection chambers	10
2.2.4 Scintillators	12
2.2.5 Tracking calorimeters	12
3 The SuperNemo demonstrator	14
3.1 The SuperNemo demonstrator	14
3.1.1 Comparison with Nemo3 experiment	14
3.1.2 Experimental design	14
3.1.3 Sources	14

3.1.4	Tracker	14
3.1.5	Calorimeter	14
3.1.6	Calibration systems	14
3.1.7	Control Monitoring system	14
3.1.8	Electronics	14
3.2	The SuperNemo software	14
3.2.1	Simulation	14
3.2.2	Reconstruction	14
4	Analysis tools	15
4.0.1	Internal probability	15
4.1	Simulations	16
4.1.1	Modifications of simulation software	16
4.1.2	Internal background simulations	16
4.1.3	$0\nu\beta\beta$ simulations	16
5	Time difference	17
5.1	Principle and goal	17
5.1.1	Internal conversion	17
5.2	Analysis	18
5.2.1	Topological cuts	18
5.2.2	Exponentially modified Gaussian	18
5.2.3	Results	18
5.3	Conclusion	18
6	Characterisation of the calorimeter resolution	20
6.1	Calibration with a Cobalt source	20
6.1.1	Experimental setting and goal	20
6.1.2	Data taking at LSM	20
6.1.3	Analysis	20
6.1.4	Results	20
6.2	The Light Injection System	20
6.2.1	Principle	20
6.2.2	Time resolution of optical modules	20
7	Detector commissioning	22
7.1	Reflectometry tests	22
7.1.1	Principle and goal	22
7.1.2	Data taking at LSM	23
7.1.3	Pulse timing: controlling cable lengths	23
7.1.4	Correction on event times	25

7.1.5	Checking the pulse amplitude attenuation	26
7.1.6	Checking the constructor signal velocity in cables	26
7.1.7	Studying influence of CFD on the signal timing study	26
7.1.8	Pulse shape analysis	26
7.1.9	Results	26
7.2	Calibrating the electronics	26
7.2.1	Principle	26
7.2.2	Measuring the time offset of front end boards	26
7.2.3	Results	26
Conclusion		28
Bibliography		29

Chapter 7

Detector commissioning

By the end of 2019, the commissioning of the SuperNEMO demonstrator has begun and first calorimeter data were taken.

To clarify, we give some common terms used in the detector assembly. The calorimeter of SuperNEMO is segmented in 712 optical modules (OM), each composed by a coupling between a photomultiplier tube (PMT) and a polystyrene scintillator (see sec. 3.1.5 for more details). The divider of a PMT is connected to 2 cables, one providing the high voltage (HV), the other one, called signal cable, is a coaxial cable collecting and transporting the charge provided by the PMT.

By the summer 2020, the SuperNEMO demonstrator will be encapsulated in an anti radon tent ([abbrev?](#)). The so called *patch panel* (PP) will insure passage of cables from inside, to outside the anti radon tent, therefore doubling the amount of cables needed for the calorimeter. We commonly talk about *internal* cables (from detector to patch panel) and *external* cables (from patch panel to electronics). Consequently, regarding only the calorimeter part, 2848 cables were cut, assembled, connector-mounted, transported and installed at Modane. Then checking cables condition is mandatory to control and eventually fix the cables.

7.1 Reflectometry tests

7.1.1 Principle and goal

Taking into account the final demonstrator design, each coaxial cable length were determined, then cables were cut and labelled in LAL, Orsay. To check if the cables were cut at right length and if no inversions were made at Modane when connecting cables, we want to verify each cable length after installation. To do so, a channel at electronic boards send a pulse, called *primary* pulse, in the connected cable. The signal will travel from electronics to the PMT through this coaxial cable. As the PMT is not alimented (the HV is turned off during this data taking), the impedance at PMT is infinite, and the signal reflects at PMT

divider. Then the signal travels back from the PMT to the channel at electronic boards, where it will be recorded by the acquisition. We called this recorded back pulse *secondary* pulse. To analyse the shape and arrival time of those secondary pulses will allow us to check the coaxial cable conditions and control their lengths.

7.1.2 Data taking at LSM

Explain the pulse sending principle with Jihane's documentation

7.1.3 Pulse timing: controlling cable lengths

After all cables were transported to Modane, to determine precisely each coaxial cable length is important for three reasons:

- to control if no inversions were made during calorimeter cabling: all external coaxial cable is 7 meters-long (the distance between electronics and patch panel being the same for all channels), but internal cables length have been adapted to fit the distance from the patch panel to each optical module;
- to check if cables were cut at right length;
- to estimate the delay of signal due to cable lengths: the velocity of electrons in cables has a regular value that delays the signal coming from the PMT. This time delay depends on the cable length and has to be characterised for each electronic channel.

In order to do this, we determine the difference between primary pulse and secondary pulse times. Knowing the velocity of electrons in coaxial cables, we can deduce the corresponding cable length. This measure is repeated for each PMT, allowing us to characterise all coaxial cables.

The propagation velocity of electrons in coaxial cables, v_p , is a parameter given as a fraction of the light speed in vacuum, c , as

$$v_p = \frac{1}{\sqrt{\epsilon}},$$

with ϵ the dielectric constant of the material. For the coaxial cables chosen for the demonstrator, this velocity is $0.69c$.

We define the time of a pulse with a Constant Fraction Discriminator (CFD) parameterised by the fraction f , as represented in fig. 7.2.3. **expliquer CFD dans texte** We studied the influence of this fraction on the time measurement precision (see Sec. 7.1.7). In the following, we use $f = 40\%$. The cable length \mathcal{L} is therefore defined as $\mathcal{L} = 0.5 \mathcal{T} v_p$, with \mathcal{T} the round trip time from electronics to PMT divider, defined as

$$\mathcal{T} = \langle t_{\text{secondary pulse}} - t_{\text{primary pulse}} \rangle_p, \quad (7.1)$$

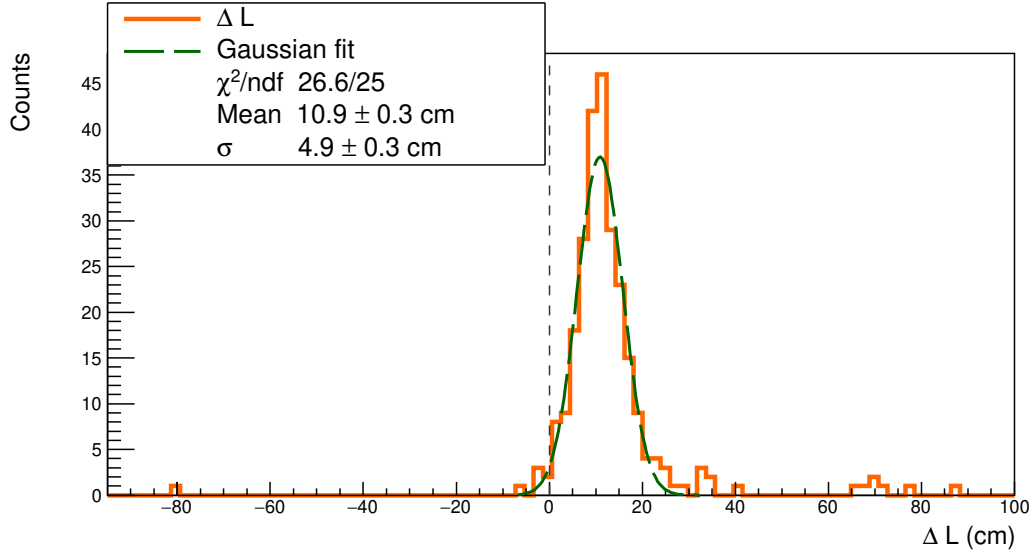


Figure 7.1: The distribution of difference between measured length (by reflectometry) and expected length is displayed in orange plain line. The gaussian fit (red dashed line) has a mean of 10.9 ± 4.9 cm.

$\langle \rangle_p$ being the average over all pulses sent in one cable, and t_i the time of pulse i . We repeat this operation for all electronic channels so all cables are controlled and characterised. A study was also performed to experimentally confirm electron celerity in the used coaxial cables (see Sec. 7.1.6).

The principal aim of this study is to control if cables were correctly cut, following the initial design. Therefore, we define l_j^d as the initial designed length for a given cable j , and l_j^m the cable length measured by reflectometry for a cable j . Hence the length difference ΔL_j for a cable j is defined as:

$$\Delta L_j = l_j^m - l_j^d. \quad (7.2)$$

On Fig. 7.1.3 is displayed the distribution ΔL for all the measured coaxial cables. In hypothetical perfect conditions, all the cables j should have the designed length, in other words, $l_j^d = l_j^m$. Consequently the ΔL distribution should be a Dirac peak centered at 0, as materialised by the black dashed line. However, in real conditions, the measured length can be different from the designed one, leading to a gaussian distribution plotted in orange plain line. A gaussian fit (green dashed line) performed on this ΔL distribution point out a σ value of 4.9 cm, revealing the precision of the cutting device. The mean value of the gaussian fit is also interesting, with 10.9 cm, meaning that cables are longer than expected in average. This may reveal a bias coming from the device used to cut the cables. On Fig. 7.1.3 is plotted the length difference ΔL with the initial designed length l^d

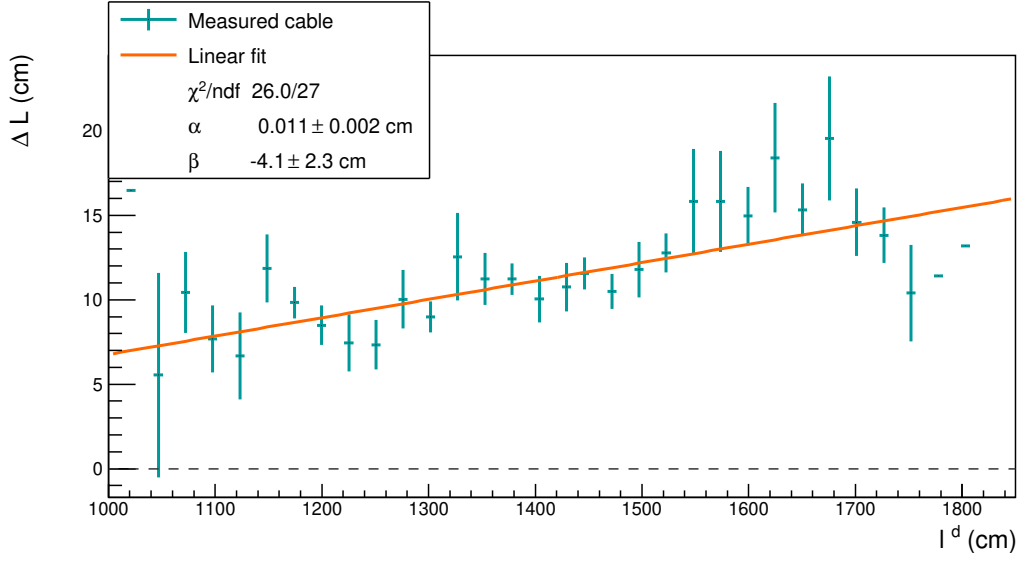


Figure 7.2:

(greened blue). A linear fit parameterised by $y = \alpha x + \beta$, is displayed in orange plain line. The y -intercept of this linear fit, represented by the parameter β , shows that the cutting device systematically take away -4.1 cm of each cable. Besides, the slope of the linear fit, α , reveals a slight bias of the cutting device, adding 1 cm every meter of cable. This bias would have been a problem with a negative slope, in other words, if measured cable lengths were systematically smaller than the designed ones, leading to eventual connection issues to PMT. However, we can notice that some cables have been cut shorter, one of them being 80 centimeters shorter than expected. Hopefully, this cable were checked at LSM, showing it was successfully connected to PMT despite this deficit.

This study allowed us to control and record the lengths of all coaxial cables installed on the SuperNEMO demonstrator at LSM. In addition, reflectometry also aimed at checking the cable condition by performing waveform shape analysis on secondary pulses.

Rq: controlling the length do not include that the cable is connected (reflection can occur at the end of the cable).

7.1.4 Correction on event times

The main goal of this study was to check the lengths of coaxial cables. We can also use the results to correct the time of recorded events. Given that what we later define as an *event* is firstly an electric signal, we should take into account the time for the signal to travel through cables. This become possible with the reflectometry study we performed.

Knowing real lengths of cables and using the celerity of the signal, we deduce the time needed for the signal to travel from one given PMT divider to the electronics. Then we can correct event times.

7.1.5 Checking the pulse amplitude attenuation

When the signal travels in a cable, its amplitude is attenuated. Then, another test for controlling the cable condition is to check if this attenuation matches the expectations (i.e. the value given by constructor). We define the amplitude of a pulse as the maximum of this pulse, compared to the baseline. The attenuation \mathcal{A} of a given cable is then defined as $\mathcal{A} = \langle A_{\text{secondary pulse}} - A_{\text{primary pulse}} \rangle_p$, A_i the amplitude of the pulse i . A map summarising the attenuation for each cable is presented.

7.1.6 Checking the constructor signal velocity in cables

As we want to check the celerity of signal given by Axon, we used 3 cables of different lengths (see Fig. 7.2.3). Knowing the length of a cable, we determine the time needed for the signal to make a round trip in the cable, and conclude about the celerity of signal in each cable. We found that the mean celerity on the 3 cables is 0.7 c, a bit greater than the celerity given by Axon of 0.69 c.

7.1.7 Studying influence of CFD on the signal timing study

7.1.8 Pulse shape analysis

7.1.9 Results

7.2 Calibrating the electronics

7.2.1 Principle

7.2.2 Measuring the time offset of front end boards

7.2.3 Results

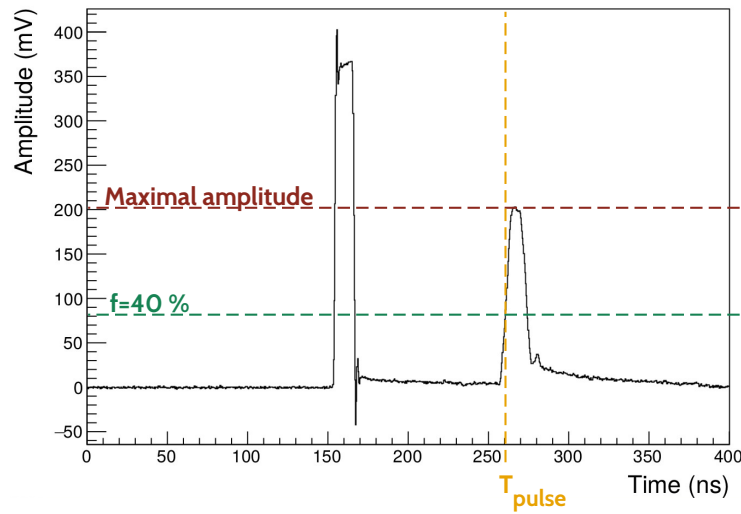


Figure 7.3: In black is an example of a waveform with primary pulse (left) and secondary pulse (right). A representation of time CFD is given for the secondary pulse. Its maximal amplitude (red dotted line) and its fraction for $f = 40\%$ (green dotted line) are displayed. The time T_{pulse} (orange dotted line) represents the time of the secondary pulse calculated with a CFD at $f = 40\%$.

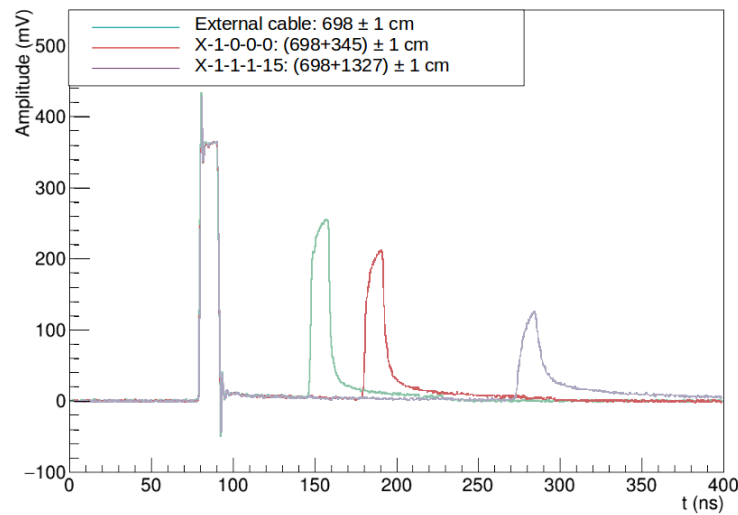


Figure 7.4: Primary and secondary pulses for a 698 ± 1 cm cable (green), a 1043 ± 1 cm cable (red) and a 2025 ± 1 cm cable (grey).

Bibliography

- [1] M. et al. Agostini. Probing majorana neutrinos with double- β decay. *Science* 365, 1445, 2019.
- [2] S.I. et al Alvis. Search for neutrinoless double-beta decay in ^{76}Ge with 26 kg-yr of exposure from the majorana demonstrator. *Phys. Rev. C*, 100, 2019.
- [3] O. et al. Azzolini. First result on the neutrinoless double- β decay of ^{82}Se with cupid-0. *Phys. Rev. Lett.*, 120:232502, Jun 2018.
- [4] C. et al. Alduino. First results from cuore: A search for lepton number violation via $0\nu\beta\beta$ decay of ^{130}Te . *Phys. Rev. Lett.*, 120:132501, Mar 2018.
- [5] J. B. et al. Albert. Search for neutrinoless double-beta decay with the upgraded exo-200 detector. *Phys. Rev. Lett.*, 120:072701, Feb 2018.
- [6] A. et al. Gando. Search for majorana neutrinos near the inverted mass hierarchy region with kamland-zen. *Phys. Rev. Lett.*, 117:082503, Aug 2016.